Hindawi
Advances in Materials Science and Engineering
Volume 2019, Article ID 3151823, 12 pages
https://doi.org/10.1155/2019/3151823

*Research Article*

# Compilation and Application of UMAT for Mechanical Properties of Heterogeneous Metal Welded Joints in Nuclear Power Materials

**He Xue**,[1] **Yueqi Bi**,[1] **Shuai Wang**,[1,2] **Jianlong Zhang**,[1] **and Siyu Gou**[1]

[1]*School of Mechanical Engineering, Xi'an University of Science and Technology, Xi'an 710054, China*
[2]*College of Engineering, Design and Physical Sciences, Brunel University, London UB8 3PH, UK*

Correspondence should be addressed to He Xue; xue_he@hotmail.com, Yueqi Bi; 17205020034@stu.xust.edu.cn, and Jianlong Zhang; 16105301004@stu.xust.edu.cn

Received 15 July 2019; Accepted 11 October 2019; Published 22 November 2019

Academic Editor: Fuat Kara



For the problem of mechanical properties of heterogeneous dissimilar metal welded joints, when analyzed by the finite element method, it is usually simplified into a "sandwich" material structure model. However, the mechanical properties of materials in different regions of the "sandwich" material mechanics model are different, and there will be mutations at the material interface. In order to accurately describe the mechanical properties of welded joints, the constitutive equations of dissimilar metal welded joint materials were compiled, and the constitutive equations of inhomogeneous materials whose material mechanical properties were continuously changed with space coordinates were established. The ABAQUS software was used to establish the "sandwich" model and the continuous transition model. The model is used to compare and analyze the crack tip stress distribution of different yield strength mismatch coefficients. The results show that the continuous transition material model eliminates the mutation of the "sandwich" model at the material interface and achieves the continuous change of the mechanical properties of the material. For the longitudinal crack, under the influence of different mismatch coefficients, the crack tip stress field of the transitional material model is deflected toward the low yield strength side. The compilation of constitutive equations for continuous transition materials of dissimilar metal welded joints provides a basis for the safety evaluation of dissimilar metal welded joints.

## 1. Introduction

Damage and defect problems are important factors affecting material processing and structural life [1–3]. The welded joint is a complex heterogeneous structure composed of the base material, weld material, the weld fusion zone, and the heat affected zone. The welding process is a very complicated metallurgical process. The material of the structure, the temperature, and other dramatic changes are very likely to cause pores, cracks, and complex residual stress fields [5–7]. Because of the welding joints' extensive existence in the key components and structures of nuclear power plants, after the failure of defects, the safe operation of nuclear power plants will cause immeasurable losses. Therefore, structural integrity assessment of important components and structures in nuclear power plants is critical. Due to the particularity of the welding process, the mechanical properties of the welded joints are not uniform and the metallographic changes of the materials, the discontinuity of the structure, the variation of the mechanical field, and the evaluation of the service life as well as the safety of the structure have always been the focus of scholars and engineers. Yang et al. [7, 8] investigated the effect of the elastic response of austenitic behavior of austenitic stainless steel, the orientation of crystal orientation, and the grain boundary (GB) dip angle under constant displacement by means of numerical simulation. The results showed that the larger the difference in the orientation of the twin crystal, the greater the strain inconsistency of the twin crystal. In addition, intergranular stress corrosion cracking (IGSCC) is closely related to crystal orientation. And the

grain size effect is independent of the grain size. Subramanian et al. [9] performed a number of experiments to investigate the effect of the mechanism of premature failure of bimetal welds, which are caused by the close proximity of the ferrite (BCC) and austenite (FCC) interfaces. The results revealed that premature failure depends on the initial carbide distribution of the zone. Papadioti et al. [10] developed a version of an isotropic elastoplastic damage model that relied on the third constant J(3) of the stress deflector. The model is suitable for rate-independent and rate-dependent (viscoplastic) models. Thamburaja et al. [11] derived the three-dimensional thermodynamics-based finite deformation constitutive theory based on velocity form as well as the calculation method of damage and fracture of nonlinear viscoelastic materials.

In order to ensure the safety of nuclear power plants, low-alloy steels, austenitic stainless steels, and nickel-based alloys are widely used in light water reactor structural materials. The pressure vessel in the reactor is made of low-alloy steel such as SA-508 C1.2, SA-508 C1.3 and SA 533 Gr.B Cl.l, and a layer of stainless steel is welded on the inner surface to improve its corrosion resistance [12–14]. In the reactor primary circuit water circulation system, the pipe material is stainless steel, and in order to ensure the quality of the welded joint, the welding metal is made of nickel-based alloy, which causes dissimilar metal welding at the joint of the pressure vessel and the main pipe.

When using the finite element method to study the mechanical properties of dissimilar metal welded joints, the dissimilar metal welded joints are mainly simplified into the "sandwich" material structure model [15], that is, the welded joints are partitioned, and the material parameters of various parts are different but constant parameters, that is, just like a sandwich. There is a sudden change in material properties at the junction. This model has certain limitations on the structural integrity safety evaluation of heterogeneous metal welded joints on nuclear power safety terminal.

In order to accurately describe the complex mechanical field of heterogeneous metal welded joints on nuclear power safety terminal, the effects of different yield strength mismatches on crack tip stress-strain distribution law are analyzed, and the problem of material property mutation at the boundary of different materials of "sandwich" material structure model is solved. The user subroutine of continuous transition constitutive equation, which performed the inhomogeneous material mechanical properties of dissimilar metal weld joint, has been written by ABAQUS User Defined Material Mechanical Behavior (UMAT). In other words, the constant elastic modulus and yield strength are replaced by function, which the material property values changed with space coordinates, and then the continuous change of elastic modulus and yield strength parameters is realized. Compared with the "sandwich" material structure model, the cracked tip stress field distribution of different yield strength mismatch coefficients of dissimilar metal welded joints is analyzed. The regular influence provides basic material performance data for the subsequent integrity assessment of the heterogeneous metal welded structure at the safety terminal.

## 2. UMAT Compilation

*2.1. Formula Derivation.* In order to meet the high temperature and high pressure corrosion environment during nuclear power plant operation, austenitic stainless steel and nickel base alloy steel with good ductility and plasticity are widely used in nuclear power bearing equipment [16]. Therefore, the stress-strain relationship in the elastic phase is linear. When the Mises stress exceeds the yield limit, the stress-strain relationship of the material changes as a power hardening law. A piecewise function is used to express the stress-strain relationship of the material, as in

$$\begin{cases} \sigma = E\varepsilon_e, & (\overline{\sigma} < \sigma_s), \\ \sigma = A\left(\varepsilon_p\right)^n + \sigma_s, & (\overline{\sigma} < \sigma_s). \end{cases} \tag{1}$$

In the equation, $\sigma_s$ is the yield strength of the material, $\varepsilon_e$ is the elastic strain, $\varepsilon_p$ is the plastic strain, and $n$ is the hardening index. $\overline{\sigma}$ is the MISES equivalent stress; when the material equivalent stress is lower than the material yield limit, the material is deformed elastically, the stress-strain relationship is $\sigma = E\varepsilon_e$, $E$ is the elastic modulus, and when the material equivalent stress is higher than the material yield limit, the material is deformed plastically, and the plastic stress-strain relationship is $\sigma = A(\varepsilon_p)^n + \sigma_s$; in order to ensure the continuity of the material constitutive equation, in the plastic stage, the tangent stiffness at yield strength value is equal to the tangent slope of the elastic stage (that is, the elastic modulus), and the tangent slope of the plastic stage material is given as

$$\frac{\mathrm{d}\sigma}{\mathrm{d}\varepsilon_p} = An\left(\varepsilon_p\right)^{n-1}. \tag{2}$$

The plastic strain at the yield point is $\varepsilon_p = \sigma_s/E$; in order to ensure that the elastic section curve of the material is continuous with the tangent line of the plastic section curve, the tangent slope of the plastic section curve should be equal to Young's modulus $E$, that is, the tangent stiffness at the yield point of the plastic stage material is $\mathrm{d}\sigma/\mathrm{d}\varepsilon_p = E$, and bringing it into equation (2), we can get the expression of A:

$$A = \frac{E^n}{n\left(\sigma_s\right)^{n-1}}. \tag{3}$$

In this paper, the standard tensile test (CT specimen) is taken as the research object. The relationship between the CT specimen and the material of the welded joint is shown in Figure 1. The crack tip is the coordinate origin and the crack propagation direction is the positive direction. The Cartesian coordinate system is established in units of mm.

Regardless of the complex residual stress field at the weld, it is assumed that the mechanical properties of the material are continuously transitioned from the base metal to the weld along the normal direction of the material boundary. The normal material boundary is a straight line, and the expression of $f(x, y)$ is

$$f(x, y) = ky + x. \tag{4}$$

The parameter $k$ is the slope of the line and is related to the angle $\theta$ between the mechanical properties of the

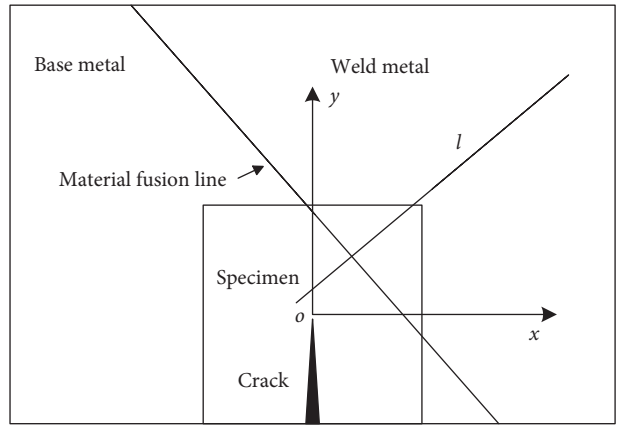


Figure 1: Relationship between the change law of mechanical properties and space coordinates.

material and the crack, $k = \tan\theta$. The parameter $k$ is the slope of the line and is related to the angle between the mechanical properties of the material and the crack. Replace the modulus of elasticity and yield strength with a function of space coordinates, as in

$$\begin{cases} E(x, y) = K_1(y\tan\theta + x) + E_0, \\ \sigma_s(x, y) = K_2(y\tan\theta + x) + \sigma_{s0}, \end{cases} \tag{5}$$

where $K_1$ and $K_2$ are the elastic modulus proportional coefficient and the yield strength proportional coefficient, respectively, in units of MPa/mm. When $K_1$, $K_2$ is 0, the constitutive equation can be used for numerical simulation of uniform materials. $E_0$ is the modulus of elasticity constant term, and $\sigma_{s0}$ is the yield strength constant term.

The constitutive relation of the above materials is compiled into the ABAQUS user subroutine in FORTRAN language. In the UMAT subroutine, there are five input parameters, namely elastic modulus $E_0$, Poisson's ratio $\mu$, yield strength $\sigma_{s0}$, elastic modulus proportional coefficient $K_1$, and yield strength ratio $K_2$. The coefficient and the mechanical product properties change the direction and the angle between the cracks $\theta$.

*2.2. Welded Joint Model Establishment.* Figure 2 shows the schematic diagram of the welded joint of the safety terminal [17]. The finite element model is shown in Figure 3. The structure is simplified into a two-dimensional plane strain model with a dimension of 100 mm × 35 mm. The coordinate system is located at the lower left corner of the structure, the left side of the model is fixed, and the horizontal displacement load is applied to the right side by 0.5 mm.

The simplified structural finite element model has a total of 3000 four-node plane strain elements.

The elastic modulus of dissimilar metal welded joint material is 180 GPa, and Poisson's ratio is 0.3. The hardness of the welded joint near the weld line is significantly greater than the hardness of the base metal and the weld metal, and the hot melt zone (HFZ, heat affected zone and fusion zone) affected by the weld heat has obvious structural and performance heterogeneity [18]. In order to eliminate the mechanical property abruptness of the material interface, the cosine function is used to fit the yield strength of the continuous transition model material in sections and change along the $x$ direction, as in

$$\sigma_s = \begin{cases} 400, & x \in [0, 12.5), \\ -100 * \mathrm{COS}\left(2 * \dfrac{3.14}{50} * (x - 25)\right) + 400, & x \in [12.5, 25), \\ 50 * \mathrm{COS}\left(2 * \dfrac{3.14}{50} * (x - 50)\right) + 550, & x \in [25, 37.5), \\ 500, & x \in [37.5, 62.5), \\ 50 * \mathrm{COS}\left(2 * \dfrac{3.14}{50} * (x - 50)\right) + 550, & x \in [62.5, 75), \\ -150 * \mathrm{COS}\left(2 * \dfrac{3.14}{50} * (x - 50)\right) + 600, & x \in [75, 87.5), \\ 300, & x \in [87.5, 100]. \end{cases} \tag{6}$$

When establishing a "sandwich" material structure model, the structure is divided into a plurality of regions to impart material properties, and the yield strength relationship of materials in different regions is as shown in

$$\sigma_s = \begin{cases} 400, & x \in [0, 37.5), \\ 500, & x \in [37.5, 62.5), \\ 450, & x \in [62.5, 137.5), \\ 500, & x \in [137.5, 162.5), \\ 300, & x \in [163.5, 200]. \end{cases} \tag{7}$$

*2.3. Discussion of Welded Joint Results.* Figure 4(a) shows the Mises stress contour diagram of the heterogeneous metal welded joint of the "sandwich" material structure model. It can be seen from the figure that under the same displacement load, since the material with low yield strength is plastically deformed before the material with high yield strength, the stress on both sides is less than the stress in the

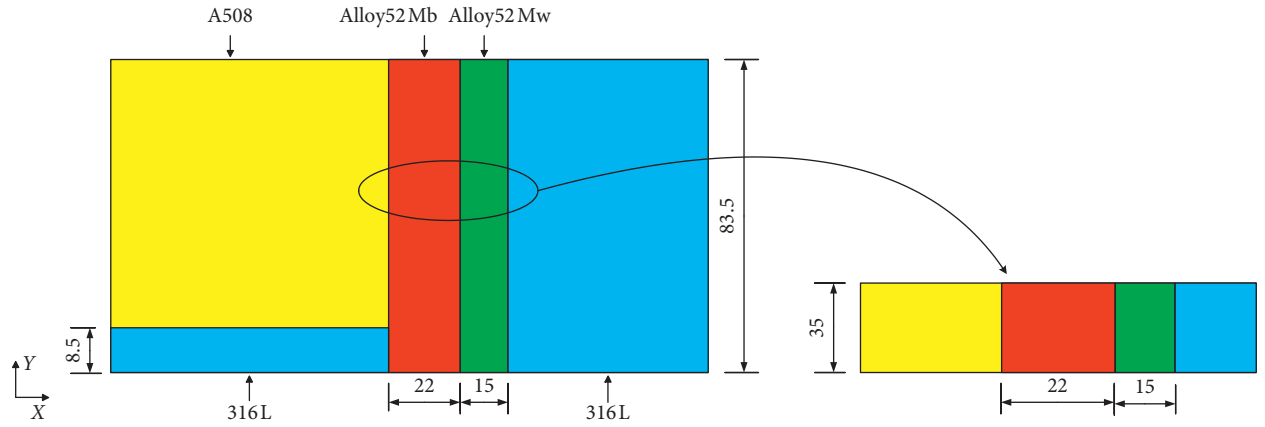


Figure 2: Schematic diagram of the welded joint of the safety terminal.

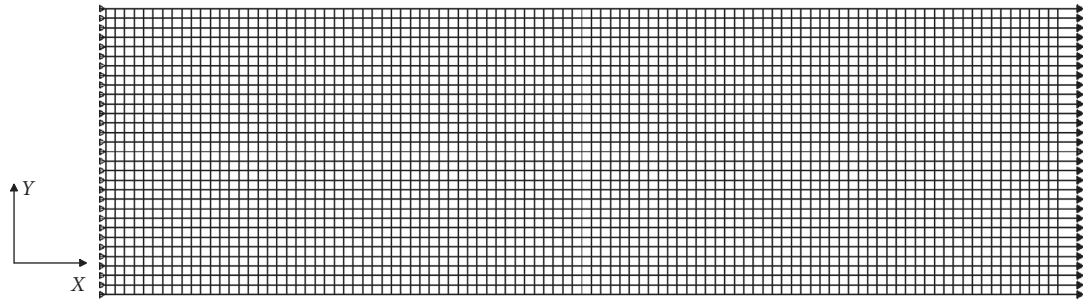


Figure 3: The finite element model of welded joint.

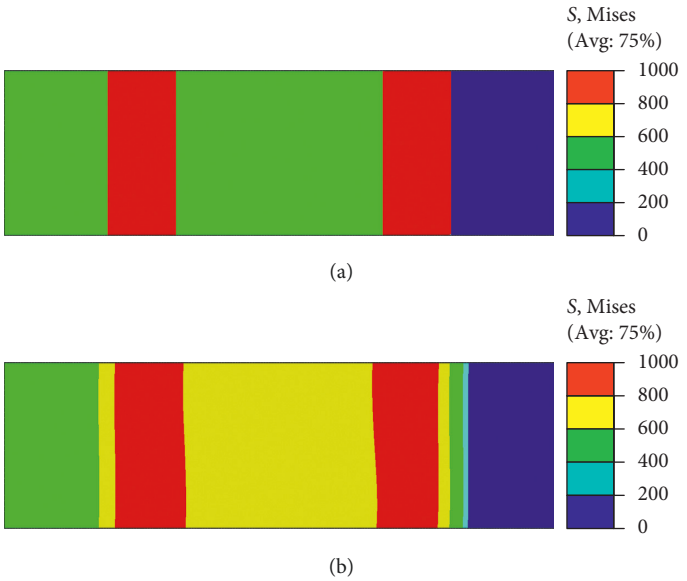


Figure 4: The Mises stress contour of the heterogeneous metal welded joint at the safety terminal. (a) The "sandwich" material structure model. (b) Continuous transition material structure model.

middle region, and the stress boundary line is located at the interface of the two materials.

Figure 4(b) shows the Mises stress contour diagram of the heterogeneous metal welded joint of the continuous transition material model. The continuous transition model has a gradual transition of stress, and there is no "intermittent" phenomenon; under the same displacement load, the material with low yield strength is plastically deformed before the material with high yield strength, and the stress on both sides is less than the stress in the middle region.

It can be seen from Figures 4(a), 5, and 6 that the "sandwich" material structure model and the continuous transition material structure model can reflect the mechanical properties of dissimilar metal welded joints in some cases. However, the mises and the equivalent plastic strain curves of the "sandwich" material structure are not continuous that will affect the accuracy of the results.

However, the continuous transition model stress and the equivalent plastic strain, in Figures 4(b), 5, and 6, change gradually. Compared with the "sandwich" material structural model, the sudden change of the curve of the continuous transition model does not exist, that is, the material properties of the continuous transition model continuously change with the x coordinate.

## 3. Static Crack Model Establishment

As shown in Figure 7, the pressure vessel is piped to the low carbon steel [19] A508, and the nozzle and the 316L stainless steel pipe are welded by a multipass nickel Alloy 52 M. The surfacing layer and butt weld solder are both nickel and Alloy52 M, but the chemical element content changes during the welding process. Alloy52 Mb and Alloy52 Mw appear on both ends of the weld. The stress corrosion cracking process and the microstructure and hardness distribution are uneven according to the welded joint material. In the study [20], stress corrosion cracking is easy to occur at the end of the weld, so the crack is prefabricated at that place.

*3.1. Geometric Model.* At present, there are still many difficulties in the experiment of heterogeneous material structure. It is simple and easy to perform through finite element numerical simulation, and the results are reliable. In order to facilitate the analysis and calculation, a simplified model of compact tensile specimens with prefabricated crack is selected to analyze the distribution of crack tip stress field of eccentric metal welded joints. The simplified CT specimen size and crack location distribution are shown in Figure 7.

The compact tensile test (CT specimen) was used as a standard specimen for the fracture toughness test [21]. Figure 8 is a basic dimension drawing of the CT sample, where $a = W/2$, $W = 50$ mm, and $B = W/2 = 25$ mm.

*3.2. Material Model.* The safety-terminal dissimilar metal welded joint is consisting of low carbon steel A508, hot melt zone Alloy52 Mb and weld materials Alloy52 Mw and 316L [22], Young's modulus is 180 GPa and Poisson's ratio is 0.3, respectively, and the yield stress is 476, 393, 389 and 227 MPa. According to the Saint-Venant principle, the yield strength of the material at the crack tip is simplified into a linear change in the stress analysis of the crack tip. The yield strength of the local material in the continuous transition material model is simplified into a linear change; the "sandwich" material structure model is simplified into two materials.

The yield strength mismatch coefficients of the surfacing layer and the weld material relative to the parent metal are

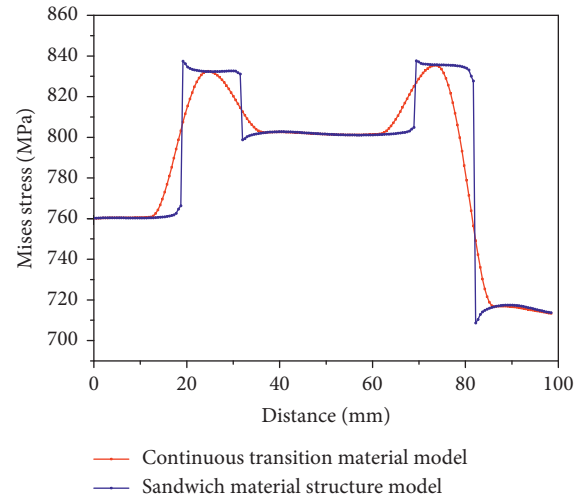


Figure 5: $X$-direction Mises stress curve of welding joint.

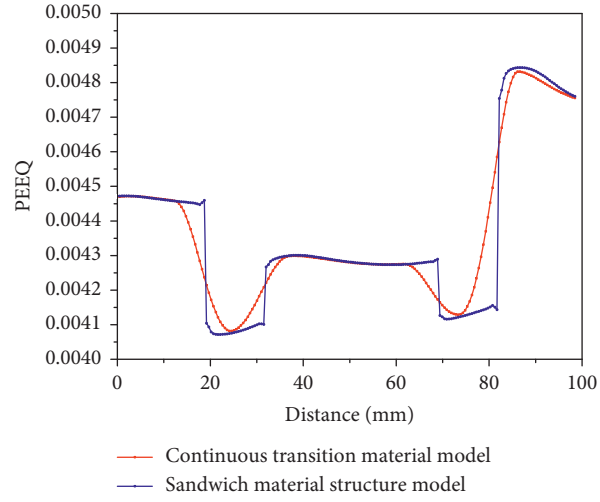


Figure 6: $X$-direction equivalent plastic strain curve of welding joint.

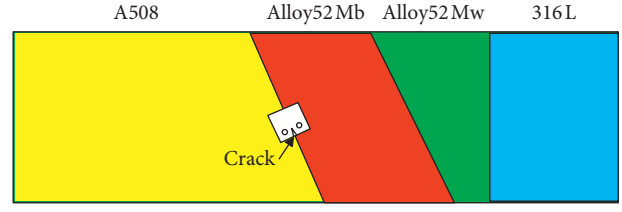


Figure 7: Schematic diagram of the crack position of the dissimilar metal welded joint at the safety terminal.

respectively determined as $M = \sigma_{s\text{Alloy52b}}/\sigma_{s\text{A508}}$, where $\sigma_{s\text{Alloy52b}}$ and $\sigma_{s\text{A508}}$ are the yield strengths of Alloy52 Mb and A508, respectively [23, 24], and the mismatch coefficient $M$ is shown in Table 1.

*3.3. Finite Element Mesh.* Figure 9 shows the finite element model of the CT specimen. The center point of the CT specimen is the hinge point. In the finite element software, the reference point is created in the center of the CT

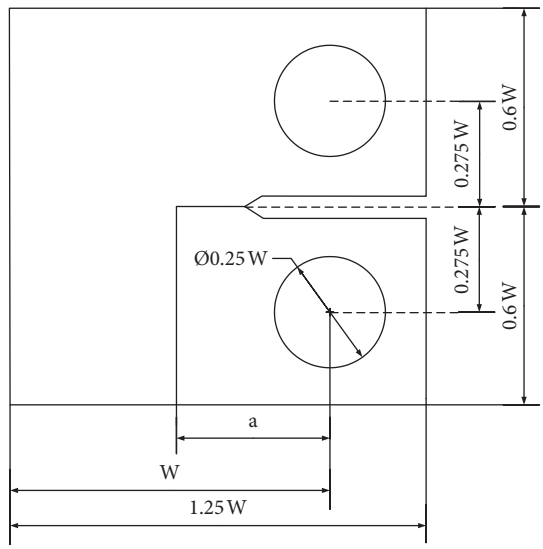


Figure 8: CT sample size schematic diagram.

Table 1: Material properties and mismatch coefficient of welded joints.

| "Sandwich" material structure model | $M$ | 0.7 | 0.8 | 0.9 | 1.0 | 1.1 | 1.2 | 1.3 |
|---|---|---|---|---|---|---|---|---|
| | A508 | 476 | 476 | 476 | 476 | 476 | 476 | 476 |
| | Alloy52 Mb | 333.6 | 393.0 | 428.4 | 476.0 | 523.6 | 571.2 | 618.8 |
| Continuous transition material model | $Y$ (mm) | $-5 \le y \le 5$ | | | | | | |
| | $\sigma_s$ ($y$) (MPa) | $14.24y + 404.8$ | $8.3y + 434.5$ | $4.76y + 452.2$ | 476 | $-4.76y + 499.8$ | $-8.3y + 523.6$ | $-14.24y + 547.4$ |
| | $\sigma_s$ (MPa) | $333.6 \le \sigma_s \le 476$ | $393 \le \sigma_s \le 476$ | $428.4 \le \sigma_s \le 476$ | 476 | $523.6 \le \sigma_s \le 476$ | $571.2 \le \sigma_s \le 476$ | $618.8 \le \sigma_s \le 476$ |

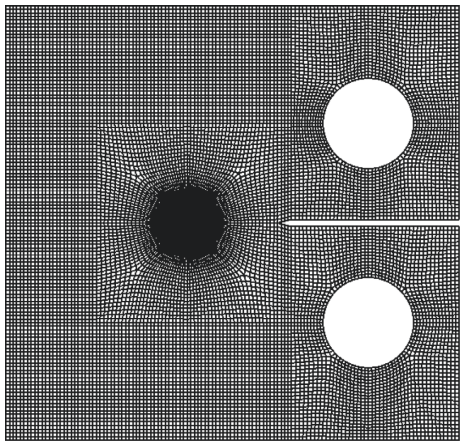

Figure 9: CT sample finite element model.

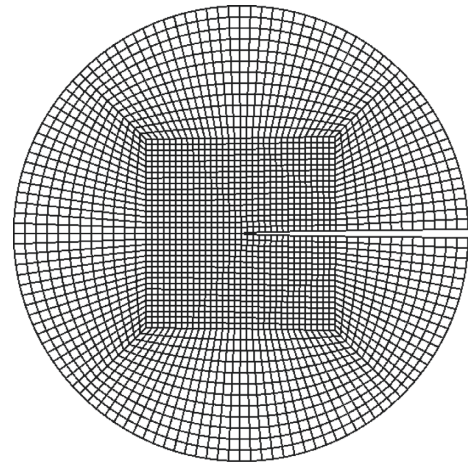

Figure 10: Crack tip local grid.

specimen, and the CT specimen is used by the coupling constraint. The inner surface of the circular hole is connected to the reference point. In the boundary condition, the reference point of one end is fixed, and the other end is applied with a load. In order to show a large plastic area in the result, a load is applied to make the crack tip stress intensity factor $K = 68\,\text{MPa}\sqrt{\text{mm}}$. Because of the limited thickness of the CT specimen, the CT specimen is simplified into a plane stress model without considering the influence of the stress in the thickness direction on the crack tip stress. As shown in Figure 10, in order to improve the calculation accuracy, the crack tip mesh is locally refined. After the mesh is refined, the finite element model mesh has a good transition and no distortion. There are 18553 four-node plane stress models.

## 4. Results and Discussions

*4.1. The Stress Field Feature of the Crack Tip.* Figure 11 shows the Mises stress contour of "sandwich" material structure model around crack tip with different mismatch coefficients

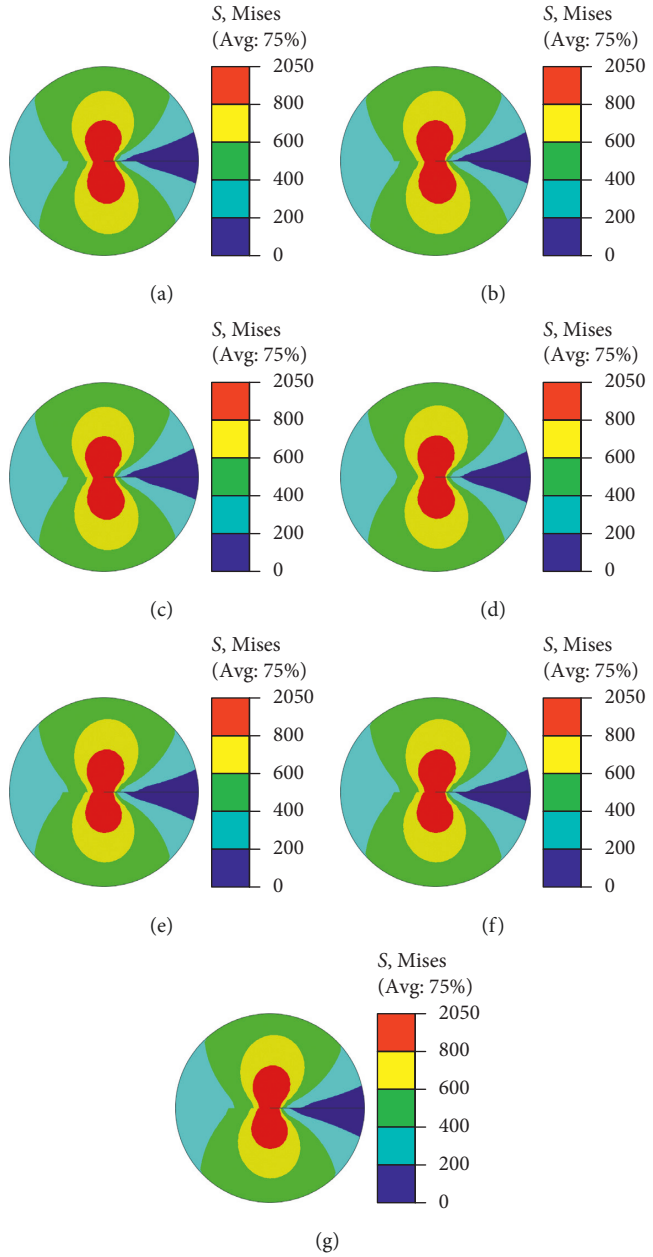


Figure 11: The Mises stress contour of "sandwich" material structure model around crack tip. (a) $M = 0.7$. (b) $M = 0.8$. (c) $M = 0.9$. (d) $M = 1.0$. (e) $M = 1.1$. (f) $M = 1.2$. (g) $M = 1.3$.

for the "sandwich" material structure model. The crack tip at the interface of 52 Mb and A508 and the geometric and material properties of the heterogeneity cause the stress to be asymmetrically distributed along the crack surface. Since the "sandwich" material structure model is a subregion that imparts material properties to the geometry, the stress values will be discontinuous at the interface. In the stress contours diagram, the discontinuity of stress is that the stress distribution area of the base metal and the stress distribution area of the weld are staggered from each other. The front and back dislocation of the stress field in different material regions is the performance of the discontinuity stress field deflection of the whole structure, and the degree of stress mutation and the crack the degree of deflection of the tip stress field are related to the material yield strength mismatch coefficient.

As shown in Figure 12, it is the Mises stress curve of "sandwich" material structure model around crack tip, where the ordinate is the stress value on the circle with the radius of 0.5 mm centered on the crack tip. The angle $\Phi > 0$ is the weld area, $\Phi < 0$ is the base material area, and $\Phi = 0$ is the material interface. As can be seen from Figures 12(a) and 12(b), there are two maximum points in the curve, and the angles corresponding to each of the maxima are equal.

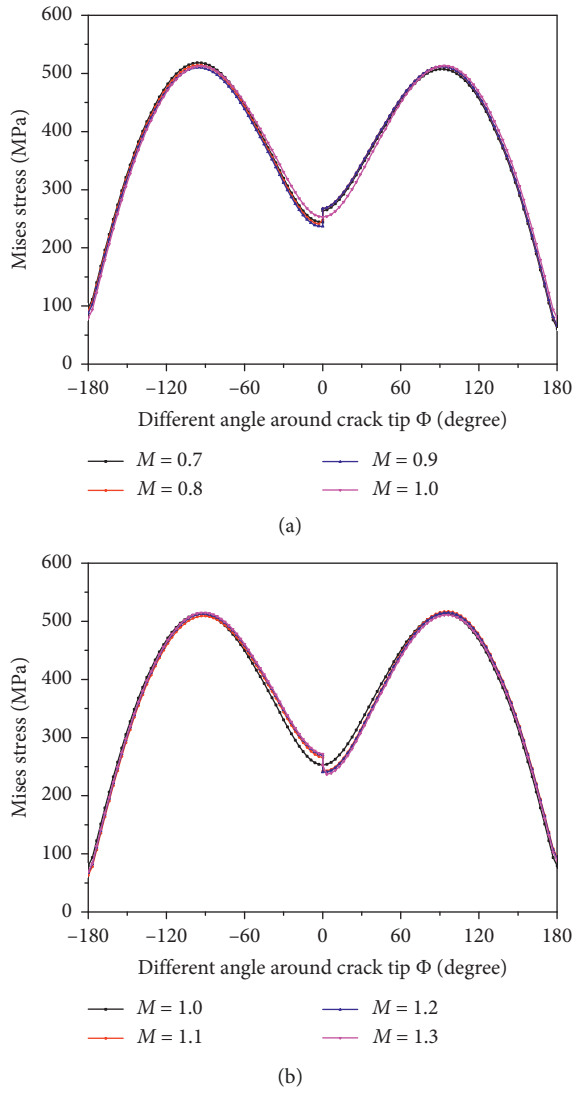


Figure 12: The Mises stress curve of "sandwich" material structure model around crack tip. (a) Mismatch coefficient $M \leq 1$. (b) Mismatch coefficient $M \geq 1$.

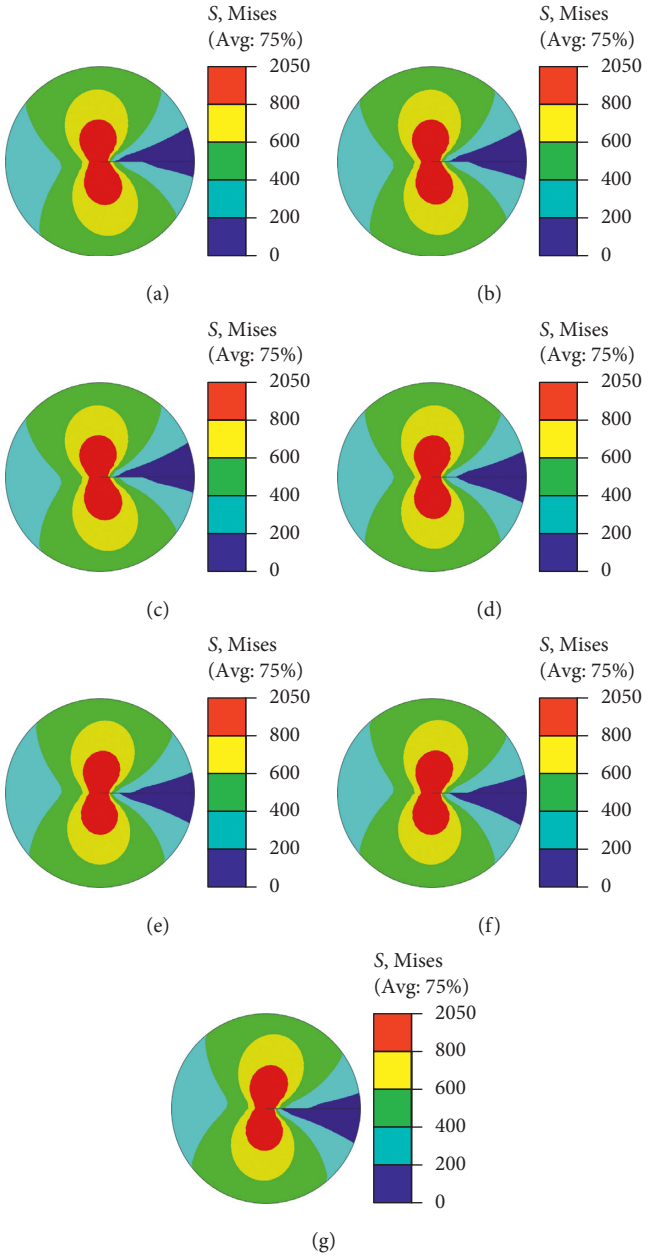


Figure 13: The Mises stress contour of continuous transition model around crack tip. (a) $M = 0.7$. (b) $M = 0.8$. (c) $M = 0.9$. (d) $M = 1.0$. (e) $M = 1.1$. (f) $M = 1.2$. (g) $M = 1.3$.

Figure 13 shows the Mises stress contour of continuous transition model around crack tip for different yield strength mismatch coefficients. It can be seen from Figure 13 that the mechanical properties of the constitutive equation of the continuously changing material using UMAT are continuously changed with the spatial coordinates. The calculation results are significantly different from the "sandwich" material structure model. The stress field stress of the continuous change model changes continuously, and there is no "fault" phenomenon of stress. The crack tip stress field is deflected integrally.

Figure 14 is the Mises stress curve of continuous transition model around the crack tip with different mismatch coefficients. It can be seen in Figures 14(a) and 14(b) that since the material mechanical properties of the continuous transition material model change continuously with the space coordinates, the curve is continuous, and all curves have two maxima points and one minima point that correspond to different angles, which is obviously different from "sandwich" material structure model in Figures 14(a) and 14(b).

When the mismatch coefficient $M < 1$, the stress gradient of the crack tip stress near the weld zone is larger than the base material stress gradient. The stress field deflects the weld zone side and the crack will expand toward the weld material.

When the mismatch coefficient $M = 1$, both the weld zone and the base zone arrive the plastic deformation simultaneously. The gradient is the same, and the stress contour map is symmetrically distributed about the crack.

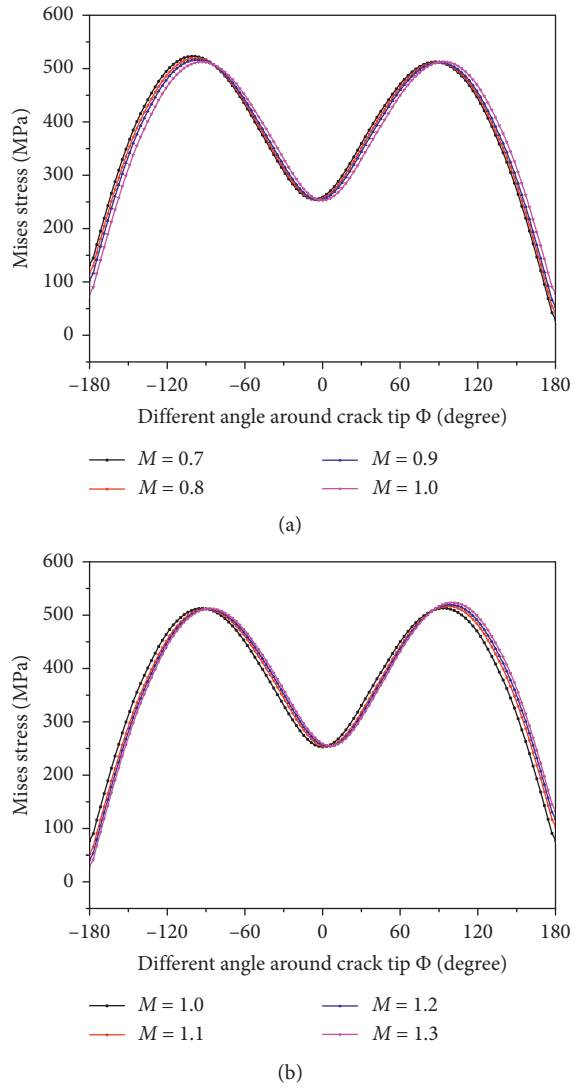


FIGURE 14: The Mises stress curve of continuous transition model around the crack tip. (a) Mismatch coefficient $M \leq 1$. (b) Mismatch coefficient $M \geq 1$.

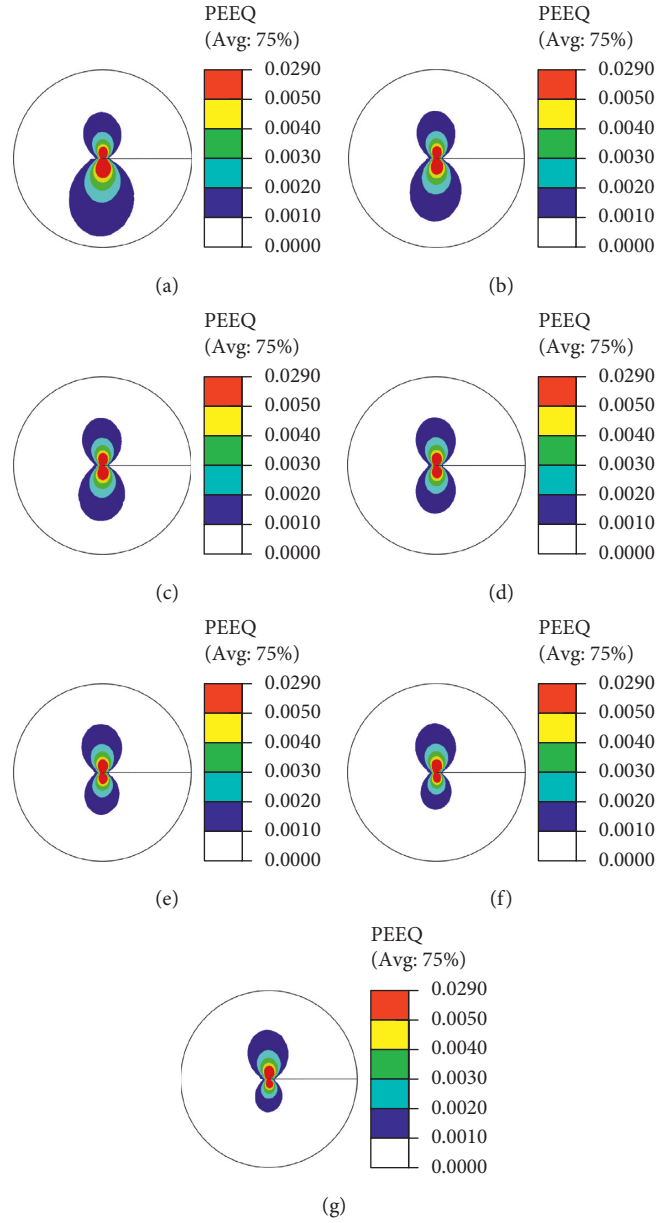


FIGURE 15: The equivalent plastic strain contour of "sandwich" material structure model around crack tip. (a) $M = 0.7$. (b) $M = 0.8$. (c) $M = 0.9$. (d) $M = 1.0$. (e) $M = 1.1$. (f) $M = 1.2$. (g) $M = 1.3$.

When the mismatch coefficient $M > 1$, the stress gradient of the weld zone is smaller than the stress gradient of the base metal region. The stress field is deflected toward the side of the base material, and the crack will expand toward the base material region.

*4.2. The Plastic Field Feature of the Crack Tip.* In the plastic analysis, the equivalent plastic strain is greater than zero, indicating that the material has yielded. Figures 15 and 16 show the local equivalent plastic strain contour and curve of the crack tip with different mismatch coefficients for the "sandwich" material structure model.

Figures 17 and 18 show the equivalent plastic strain contour and curve of the continuous transition material model with different mismatch coefficients.

When the mismatch coefficient $M < 1$, the yield strength of the weld material is lower than the base metal, and the lower yield strength of weld metal, the more large area of the equivalent plastic strain distributed. Near the weld metal side, the peak value of the equivalent strain of the weld metal is greater than the base metal. And the plastic strain field is deflected toward the weld metal zone.

On the contrary, when the mismatch coefficient $M > 1$, the yield strength of the weld metal is greater than the base metal, and the equivalent plastic strain of the base material is significantly larger than the weld metal. The gradient of the equivalent plastic in the weld zone is smaller than that in the base metal zone. The plastic zone near the lower yield strength side of the base metal is larger than the plastic zone near the higher yield strength

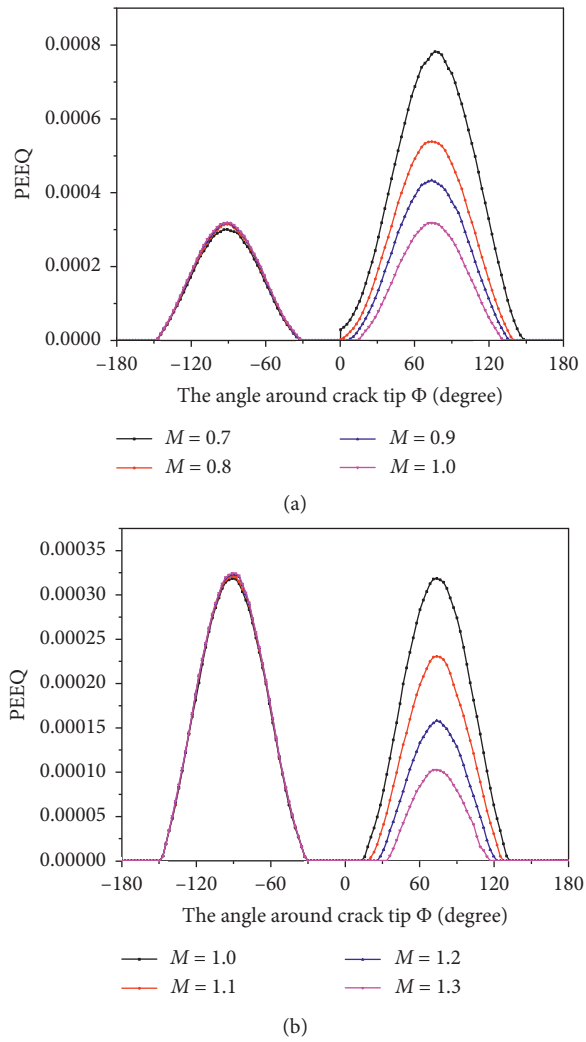


Figure 16: The equivalent plastic strain curve of "sandwich" material structure model around crack tip. (a) Mismatch coefficient $M \leq 1$. (b) Mismatch coefficient $M \geq 1$.

side of the weld side, and the entire plastic zone is deflected toward the base metal zone.

When the mismatch coefficient $M = 1$, the weld yield strength is equal to the yield strength of the material. During the loading process, the weld zone material and the parent material zone material simultaneously reach the yield strength and plastic deformation, and the equivalent plastic strain contour diagram is symmetrically distributed on the material interface.

Through the analysis of the stress and strain distribution of the crack model of the "sandwich" material structure model and the continuous transition material model, it is found that the dislocation of the stress-strain region of the "sandwich" material structure model is caused by the discontinuity of the material at the interface, and there is no continuous stress-strain mutation in the entire stress-strain region of the continuous transition material model. Under the influence of different mismatch

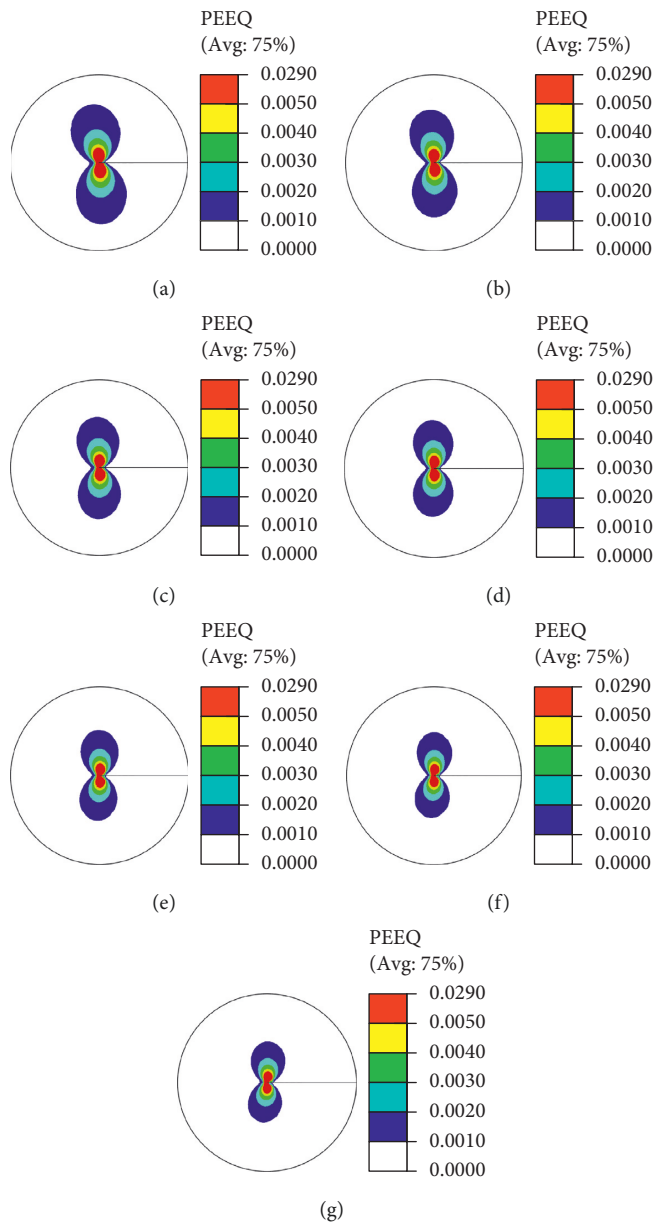


Figure 17: The equivalent plastic strain contour of continuous transition material model around crack tip. (a) $M = 0.7$. (b) $M = 0.8$. (c) $M = 0.9$. (d) $M = 1.0$. (e) $M = 1.1$. (f) $M = 1.2$. (g) $M = 1.3$.

coefficients, the crack stress strain of the two material models is always deflected toward the lower yield strength side.

## 5. Conclusions

(1) In the "sandwich" material structure model, the yield strength mismatch causes the crack tip mechanical field to be asymmetrically distributed and the crack tip stress is abruptly changed at the interface of the mechanical properties of the material. The higher yield strength side

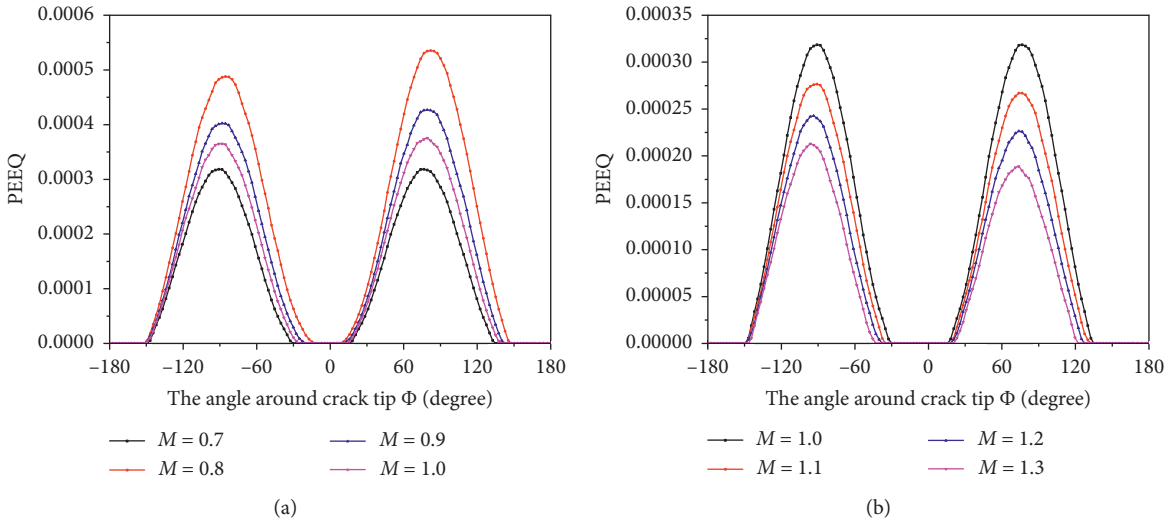


FIGURE 18: The equivalent plastic strain contour of continuous transition material model around crack tip. (a) Mismatch coefficient $M \leq 1$. (b) Mismatch coefficient $M \geq 1$.

stress and the plastic region range are smaller, and the lower yield strength side stress and plastic range are larger. A discontinuity occurs at the interface of the material. The greater the difference in the yield strength of the material, the greater the difference in the stress values on both sides of the tip.

(2) In the continuous transition model, the yield strength mismatch results in an asymmetrical continuous distribution of the crack tip mechanical field. The high yield strength side stress and the plastic region range are small. In contrast, the low yield strength side stress and the plastic region range are large. The crack tip stress field is deflected toward the low yield strength side, and the difference in material yield strength is greater as the crack tip stress field deflects toward the lower yield strength side.

(3) The "sandwich" material structure model divides the welded joint to reflect the crack propagation stress distribution of the dissimilar metal welded joint under some conditions. The shortcoming is that the stress distribution at the crack tip of the hot melt zone cannot be accurately reflected. The continuous change material mechanics model truly reflects the material properties of the hot melt zone into the model and achieves accurate calculation of the crack tip stress in the hot melt zone.

## Data Availability

(1) Previously reported material properties of 316L primary loop recirculation piping weld joint material were used to support this study and are available at http://proceedings.asmedigitalcollection.asme.org/proceeding.aspx?articleid=1627974&resultClick=3. These prior studies (and datasets) are cited at relevant places within the text as references [23].

## Conflicts of Interest

The authors declare that there are no conflicts of interest regarding the publication of this paper.

## Acknowledgments

This work was financially supported by the International Exchanges Programme Scheme project by the National Natural Science Foundation of China and the Royal Society (51811530311), the Natural Science Foundation of China (51475362), the Natural Science Foundation of Shaanxi Province (2018JQ5193), and the China Scholarship Council (201808610225).

## References

[1] Ö. Erkan, B. Işık, A. Çiçek, and F. Kara, "Prediction of damage factor in end milling of glass fibre reinforced plastic composites using artificial neural network," *Applied Composite Materials*, vol. 20, no. 4, pp. 517–536, 2013.

[2] A. Çiçek, F. Kara, T. Kivak, and E. Ekici, "Evaluation of machinability of hardened and cryo-treated AISI H13 hot work tool steel with ceramic inserts," *International Journal of Refractory Metals and Hard Materials*, vol. 41, pp. 461–469, 2013.

[3] Ö. Küçük and B. Öztürk, "Development of design geometry of aluminum fittings for healthy and safety sanitary installations," *Journal of Environmental Protection and Ecology*, vol. 18, no. 2, pp. 776–778, 2017.

[4] F.-Q. Yang, X. He, L.-Y. Zhao, X.-R. Fang, and D. Rozumek, "Effects of welded mechanical heterogeneity on interface crack propagation in dissimilar weld joints," *Advances in Materials Science and Engineering*, vol. 2019, Article ID 6593982, 10 pages, 2019.

[5] Z. P. Lu, T. Shoji, H. Xue et al., "Synergistic effects of local strain-hardening and dissolved oxygen on stress corrosion cracking of 316NG weld heat-affected zones in simulated RWR Environments," *Journal of Nuclear Materials*, vol. 423, no. 1–3, pp. 28–39, 2012.

[6] Z. Lu, T. Shoji, F. Meng, Y. Qiu, T. Dan, and H. Xue, "Effects of water chemistry and loading conditions on stress corrosion cracking of cold-rolled 316NG stainless steel in high temperature water," *Corrosion Science*, vol. 53, no. 1, pp. 247–262, 2011.

[7] F.-Q. Yang, X. He, L.-Y. Zhao, X.-R. Fang, H.-B. Zhang, and P. Lejcek, "Effects of crystal orientation and grain boundary inclination on stress distribution in bicrystal interface of austenite stainless steel 316L," *Advances in Materials Science and Engineering*, vol. 2019, Article ID 2468487, 10 pages, 2019.

[8] F.-Q. Yang, X. He, L.-Y. Zhao, X.-R. Fang, and P. Lejcek, "Effects of grain orientation on stress state near grain boundary of austenitic stainless steel bicrystals," *Advances in Materials Science and Engineering*, vol. 2018, Article ID 9409868, 10 pages, 2018.

[9] M. Subramanian, J. Galler, J. DuPont et al., "Heterogeneous creep deformation in dissimilar metal welds (DMWs)," *Materials Science & Engineering A*, vol. 749, pp. 1–13, 2019.

[10] I. Papadioti, N. Aravas, J. Lian, and S. Münstermann, "A strain-gradient isotropic elastoplastic damage model with J3 dependence," *International Journal of Solids and Structures*, vol. 174-175, pp. 98–127, 2019.

[11] P. Thamburaja, K. Sarah, A. Srinivasa, and J. N. Reddy, "Fracture of viscoelastic materials: FEM implementation of a non-local & rate form-based finite-deformation constitutive theory," *Computer Methods in Applied Mechanics and Engineering*, vol. 354, pp. 871–903, 2019.

[12] H. Ming, R. Zhu, Z. Zhang et al., "Microstructure, local mechanical properties and stress corrosion cracking susceptibility of an SA508-52M-316LN safe-end dissimilar metal weld joint by GTAW," *Materials Science and Engineering: A*, vol. 669, pp. 279–290, 2016.

[13] Y. Ueda, Y. Shi, and S. Sun, "Effects of crack depth and strength mismatching on the relation between J-integral and CTOD for welded tensile specimens," *Transactions of JWRI*, vol. 26, no. 2, pp. 133–140, 1997.

[14] Z. P. Lu, T. Shaji, F. Meng et al., "Characterization of microstructure and local deformation in 316NG weld heat-affected zone and stress corrosion cracking in high temperature water," *Corrosion Science*, vol. 53, no. 3, pp. 1916–1932, 2011.

[15] X. He, K. Ogawa, and T. Shoji, "Effect of welded mechanical heterogeneity on local stress and strain ahead of stationary and growing crack tips," *Nuclear Engineering & Design*, vol. 239, no. 4, pp. 628–640, 2009.

[16] D. W. Rathod, S. Pandey, P. K. Singh, and R. Prasad, "Experimental analysis of dissimilar metal weld joint: ferritic to austenitic stainless steel," *Materials Science and Engineering: A*, vol. 639, pp. 259–268, 2015.

[17] M. R. Mitchell, R. E. Link, Y. Sato, H. Xue, Y. Takeda, and T. Shoji, "Development of a stress corrosion cracking test methodology using tube-shaped specimens," *Journal of Testing & Evaluation*, vol. 35, no. 3, pp. 254–258, 2007.

[18] Z. Lu, X. He, H. Murakami, and T. Shoji, "Locally delaminating stress corrosion cracking growth of strain-hardened austenitic alloys in hydrogenated high temperature water environments," in *Proceedings of the ASME Pressure Vessels & Piping Conference*, vol. 6, pp. 1101–1108, Prague, Czech Republic, July 2009.

[19] H. Xue, Z. Li, Z. Lu, and T. Shoji, "The effect of a single tensile overload on stress corrosion cracking growth of stainless steel in a light water reactor environment," *Nuclear Engineering and Design*, vol. 241, no. 3, pp. 731–738, 2011.

[20] X. He, Y. Li, Y. Cui, and Z. Chen, "Analysis on micro-mechanical state at tip of stress corrosion cracking in nickel base alloy," in *Proceedings of the 2015 International Conference on Materials, Environmental and Biological Engineering*, Guilin, China, March 2015.

[21] F. Q. Yang, H. Xue, L. Y. Zhao, and X. R. Fang, "A quantitative prediction model of SCC rate for nuclear structure materials in high temperature water based on crack tip creep strain rate," *Nuclear Engineering and Design*, vol. 278, no. 8, pp. 686–692, 2014.

[22] H. Xue and T. Shoji, "Quantitative prediction of EAC crack growth rate of sensitized type 304 stainless steel in boiling water reactor environments based on EPFEM," *Journal of Pressure Vessel Technology*, vol. 129, no. 3, pp. 460–467, 2007.

[23] L. Zhao, X. He, W. Tang, and X. Fang, "Effect of welded mechanical heterogeneity on local stress and strain ahead of growing crack tips in the piping welds," in *Proceedings of the ASME Pressure Vessel & Piping Conference, No. PVP2011-57521*, Baltimore, MD, USA, July 2011.

[24] L. Xiong and Y. Zhang, "Effect of strength mis-matching on elastic-plastic deformation behaviors of welded joints with cracks," *China Mechanical Engineering*, vol. 23, no. 6, pp. 733–738, 2012, in Chinese.